RSC Advances

PAPER

View Article Online
View Journal | View Issue

Cite this: *RSC Adv.*, 2026, **16**, 6026

Tailorable conductivity of 3D PEDOT-based conductive nanostructures with pH-responsivity *via* a direct femtosecond laser writing technique

Qingbin Zhou,† Yucheng Long,† Shichao Song, * Zilan Deng, Xiangping Li and Yaoyu Cao *

Although conductive polymers such as poly(3,4-ethylenedioxythiophene) (PEDOT) are pivotal for flexible organic electronics, achieving tunable conductivity in high-resolution micro/nanoarchitectures remains a significant challenge. Conventional methods like inkjet writing and laser ablation not only offer limited resolution but also fail to provide the dynamic conductivity control required for advanced applications. To address these challenges, we developed a two-step nanofabrication strategy to produce PEDOT-based nanoarchitectures with tunable conductivities. A femtosecond direct laser writing technique was utilized to firstly create 3,4-ethylenedioxythiophene (EDOT)-based pH responsive nanostructures, and subsequently chemical oxidation was employed to convert EDOT-based nanostructures into conductive PEDOT-based ones, which enabled high-resolution conductive nanostructures with feature sizes as small as 250 nm and conductivity of 679 S m^{-1}. Additionally, the structures exhibited tunable conductivity ranging from 454 S m^{-1} (pH = 13) to 1041 S m^{-1} (pH = 1), due to the swelling/contraction of the pH responsive acrylate-functionalized derivative matrix. This work demonstrates a scalable strategy for creating high-resolution, pH-stimuli-responsive conductive polymer-based nanostructures such as PEDOT nanostructures, offering significant potential for advanced applications in nanoelectronics and biosensors.

Received 26th December 2025
Accepted 17th January 2026

DOI: 10.1039/d5ra10027e

rsc.li/rsc-advances

Introduction

Conductive organic polymers such as polyacetylene, polyaniline, polythiophene, poly(3,4-ethylenedioxythiophene) (PEDOT) and their derivatives, represent a unique class of functional polymers distinguished by exceptional properties, including plasticity, processability, light weight, low cost, and the ability to switch between conducting and insulating states, which endow them with broad application potential.[1–5] Driven by advancements in organic electronics, these conductive polymers have gained substantial traction in microelectronic devices.[6–9] While fabrication methods for devices based on conductive organic polymers have been previously reported,[10–12] certain limitations inherent to conventional approaches restrict their applicability. For example, ink formulations containing conductive organic polymers enable three-dimensional (3D) writing of microelectronic devices with diverse geometries.[13–16] However, the limitation imposed by nozzle size makes fabricating structures with micro/nano feature size extremely challenging. Alternatively, direct laser writing (DLW) using femtosecond lasers is a leading technology for achieving submicron resolution additive manufacturing, enabling the fabrication of nanoscale conductive structures.[17–23]

A fundamental challenge in the DLW-based fabrication of PEDOT micro/nanostructures lies in the inherent inability to manipulate their electric conductivities after patterning, which constitutes a primary limitation for applications requiring adaptive or responsive performance.[24–26] This constraint is further exacerbated by two critical nanofabrication challenges. First, the photopolymerization of EDOT typically requires high laser power, leading to excessive thermal accumulation and potential degradation of structural fidelity. Second, the intrinsically low crosslinking density of PEDOT hinders the realization of robust, self-supporting 3D architectures. While composite photoresist composed of poly(ethylene glycol) diacrylate (PEGDA) doped with EDOT enables the fabrication of microstructures *via* DLW with a conductivity of approximately 4 S m^{-1},[8,25] such structures are generally limited to micron-scale feature sizes. In contrast, PEDOT-based acrylate-functionalized derivatives can allow for producing micro/nanostructures *via* DLW technique with significantly high conductivity, reaching up to 2.7 × 10^5 S m^{-1},[7,8,24,27] yet this approach remains largely restricted to 2D microstructures. Importantly, across all these existing approaches, the electrical conductivities of the as-fabricated structures are fixed, lacking

Institute of Photonic Technology, College of Physics and Optoelectronic Engineering, Jinan University, Guangzhou, Guangdong 510632, China. E-mail: songsc@jnu.edu.cn; yaoyucao@jnu.edu.cn

† These authors contribute equally to this work.

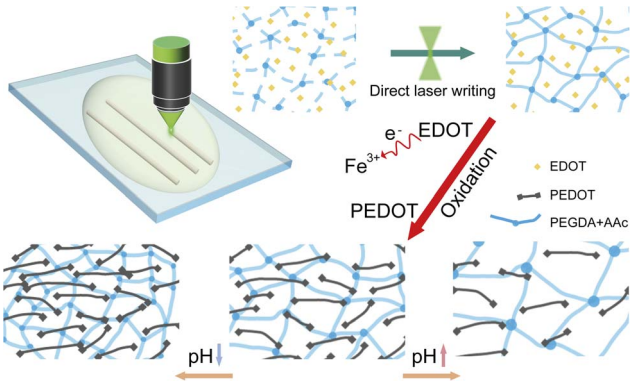

Fig. 1 Schematic of the nanofabrication of PEDOT-based nanostructures with tunable conductivities *via* hybrid direct laser writing technique.

the tunability essential for advanced functional devices. Collectively, these limitations pose a significant barrier to the development of dynamically reconfigurable or stimuli-responsive PEDOT-based micro/nanosystems.

To address these interrelated challenges, we propose a "write-then-oxidize" strategy to take advantage of high-resolution femtosecond laser direct writing technique and post-chemical oxidation, which could decouple the structuring and conductive activation steps. Therefore, it enables the fabrication of 3D micro/nanostructures with high resolution and tunable conductivities. Our approach centers on a rationally designed composite photoresist incorporating EDOT monomers within a polymer matrix of PEGDA and acrylic acid (AAc). PEGDA component ensures mechanical stability and enables complex 3D structuring, while the AAc imparts pH-responsive swelling behavior that facilitates reversible modulation of electrical conductivity. We further develop a sequential "write-then-oxidize" fabrication protocol that leverages the high chemical stability of EDOT monomers during laser writing. In the fabrication, structures are first produced using nanofabrication parameters optimized for the PEGDA/AAc matrix at substantially reduced power levels, thereby minimizing thermal damage and achieving the feature size of sub-250 nm. Subsequently, the EDOT monomers entrapped within the crosslinked polymer network are chemically oxidized to form conductive PEDOT under mild conditions, completely eliminating the requirement for high-energy *in situ* photopolymerization. This decoupled fabrication strategy effectively overcomes the critical limitations of conventional methods, enabling the realization of mechanically stable, high-resolution 3D architectures with dynamically tunable electrical properties that respond to external environmental stimuli (Fig. 1).

Experimental

Materials

3,4-Ethoxylenedioxythiophene (EDOT), poly(ethylene glycol) diacrylate (PEGDA) and acrylic acid (AAc) were purchased from Sigma-Aldrich; 2-benzyl-2-(dimethylamino)-4′-morpholinobutyrophenone (Irgacure 369) and $FeCl_3$ were purchased from TCI. All aqueous solutions were prepared using ultrapure water (Smart2Pure, ThermoFisher).

Synthesis of photoresin

First, AAc constituting 38 wt% of the total mass was added to PEGDA, which accounted for 50 wt%, and the mixture was vortexed to homogenize. Next, EDOT, making up 10 wt% of the total mass, was incorporated and thoroughly mixed. Finally, Irgacure 369, representing 2 wt% of the total mass, was added and vortexed until completely dissolved. The prepared photoresist was stored at 5 °C.

Three-dimensional DLW system

We employed a femtosecond laser (Carbide CB5, Light Conversion; 515 nm, 1 MHz repetition rate, 190 fs pulse width) as the writing beam. First, the beam was expanded and directed into an oil-immersion objective (100×, NA = 1.4, Olympus) for focusing into the photoresin. Subsequently, the desired patterns were generated by controlling a piezo stage (P-563.3CD, Physik Instrumente). The entire process was monitored in real-time *via* a CCD camera (MER-132-43U3M-L, Daheng) that provided a magnified bright-field view.

Characterizations

To assess the morphology, the structures were examined with an optical microscope (Olympus BX53), a scanning electron microscope (SEM; Apreo S, ThermoFisher), and a laser scanning confocal microscope (1C STED 75 QUAU SCAN, Abberior Instrument). The electrical conductivity of the printed line nanostructures was determined by a four-point probe system (Tech RTS-9).

Results and discussion

PEDOT, formed by the polymerization of EDOT, exhibits intrinsically low crosslinking density due to its linear chain structure, which precludes its ability to form freestanding 3D micro/nanostructures. With the aid of the photopolymerizable monomers PEGDA and AAc, EDOT can be formulated into the laser printed three-dimensional architectures. We developed a composite photoresin using EDOT, PEGDA, AAc, and Irgacure 369 at mass fractions of 10%, 50%, 38%, and 2% respectively. In order to explore the fabrication properties of the composite photoresin, a series of nanostructures were proposed including wire array, dot array, conical structure, wire-bridge structure, woodpile and polyhedral lattice framework. As presented in Fig. 2(a), wire structures were produced under different laser powers with fixed scanning speed of 30 μm s^{-1}. Wire first appeared at a laser power threshold of 0.8 mW, yielding an initial linewidth of 254 nm. This minimal feature size confirms the high spatial resolution achievable with our process. The feature size was found to increase progressively with laser power until saturation at 2.6 mW (Fig. 2(b)). A dot array (Fig. 2(c)) was fabricated with a minimum dot diameter of 335 nm at an exposure power of 1 mW and an exposure time of 50 μs, and

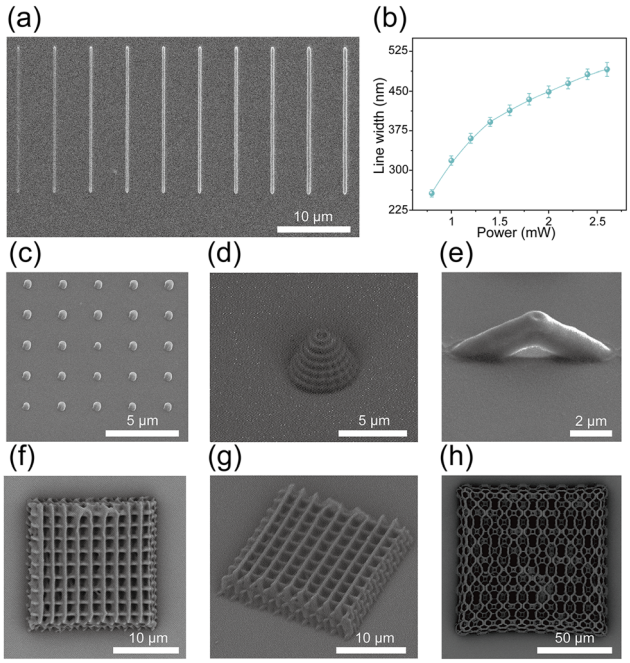

Fig. 2 The fabrication properties of laser printed structures. (a) SEM image of nanowires fabricated at different exposure powers. (b) Measured width of printed wire structures at different laser powers with scanning speed of 30 μm s^{-1} (c) SEM image of the dot array. (d) SEM image of the helical cone structure. (e) SEM image of the wire-bridge structure. (f and g) SEM images of woodpile structure at top view (f) and 45° side view (g). (h) SEM image of the polyhedral lattice framework structure.

a maximum diameter of 468 nm at 2 mW and 50 μs, demonstrating precise control over feature dimensions *via* exposure parameters. A helical cone structure (Fig. 2(d)) was fabricated at an exposure power of 2.4 mW and a scan speed of 30 μm s^{-1}, with a base diameter of 5 μm and a height of 4 μm. This complex 3D geometry showcases the method's excellent capability for creating sophisticated non-planar architectures. A wire-bridge structure (Fig. 2(e)) was also fabricated, featuring a span of 1.8 μm and a maximum height of 0.8 μm. This free-standing element highlights the sufficient mechanical strength and structural stability of the polymerized material to form suspended features. A 3D woodpile structure (Fig. 2(f) and (g)) was fabricated under an exposure power of 1.6 mW and a scan speed of 30 μm s^{-1}. The resulting structure exhibited a side length of 10 μm, a height of 5 μm, and a constituent line width of 410 nm, demonstrating robust multi-layer integration capability and structural integrity for complex 3D lattices. A polyhedral lattice framework (Fig. 2(h)) was fabricated at an exposure power of 2.6 mW, with a side length of 100 μm and height of 20 μm. This large-scale, complex 3D architecture confirms the exceptional structural stability and design flexibility achievable with our fabrication approach. These diverse structures collectively demonstrate the superior resolution, complex 3D formability, and robust mechanical properties enabled by our hybrid fabrication strategy.

The as-fabricated micro/nanostructures are endowed with electrical conductivities through oxidizing and polymerizing EDOT into PEDOT. To characterize the electrical properties achieved through chemical oxidation, large-area polymer films with a thickness of 60 μm were prepared *via* flood exposure using a 365 nm UV lamp and subsequently sectioned into 10 mm-long by 3 mm-wide strips for conductivity measurements. When these film samples were immersed in a 0.3 mol L^{-1} $FeCl_3$ solution at 40 °C, it was observed that the EDOT-based film gradually changed from its original colorless state to blue and eventually turned black, as depicted in Fig. 3(a). Visual observation of the oxidation kinetics reveals a distinct chromogenic progression correlating with PEDOT formation. The initial transparent film underwent a color change to semi-transparent blue within 0–3 minutes, signalling the onset of EDOT polymerization. The subsequent intensification of the blue color (3–9 minutes) suggests a progressive increase in PEDOT chain length and concentration. The reaction reached completion between 9-11 minutes, as the films transitioned to an opaque, black state, confirming the predominant conversion of EDOT to PEDOT and its dense integration within the PEGDA matrix.

As shown in Fig. 3(b), the oxidized film was connected to electrodes for conductivity measurements; the corresponding current–voltage (*I*–*V*) characteristics are shown in Fig. 3(c). The conductivity for different oxidation durations was calculated using the conductivity formula $\sigma = L/(R \cdot S)$, where R is the measured resistance of the film strip, and L and S represent its effective length and cross-sectional area, respectively, and the calculated conductivity values were presented in Fig. 3(d). The electrical conductivity of the polymer films exhibited a strong dependence on the duration of chemical oxidation treatment. Initially, the films were non-conductive, as the unoxidized EDOT monomers had not yet formed the conductive PEDOT network. With increasing oxidation time, EDOT progressively converted to PEDOT, imparting initial conductivity to the films. A peak conductivity of 648 S m^{-1} was achieved after 13 minutes of oxidation, indicating the formation of a relatively continuous and uniform conductive pathway by PEDOT within the PEGDA/AAc polymer network. The conductivity of PEDOT is closely related to its molecular weight and doping level, both of which

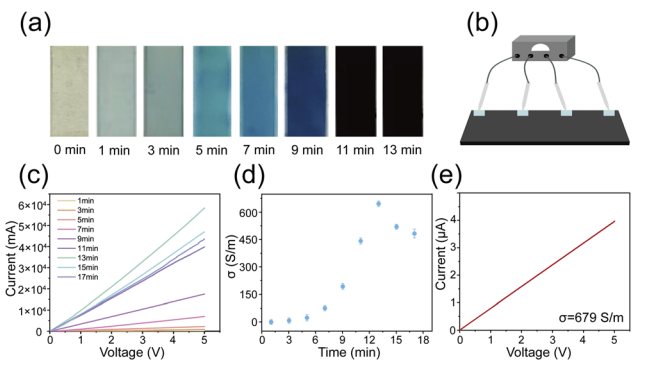

Fig. 3 Chemical oxidation renders PEDOT-based polymers conductive. (a) Color evolution of PEDOT-based polymer films with oxidation time. (b) Schematic of the four-point probe measurement for current and voltage. (c) *I*–*V* curves of the polymer films at different oxidation times. (d) Calculated electrical conductivities. (e) *I*–*V* curves of the nanowire structure after oxidation.

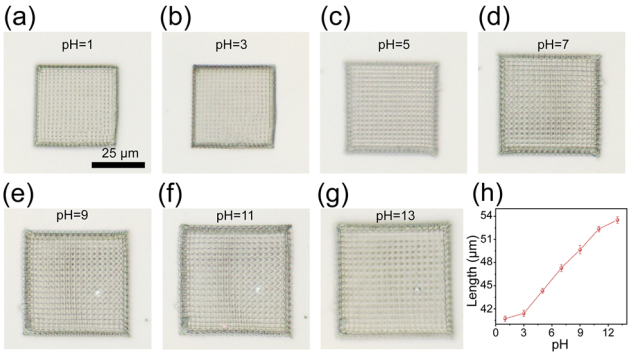

Fig. 4 Structural volume changes under different pH conditions. (a–g) optical micrographs of the woodpile structure under different pH conditions. (h) pH-dependent dimensional changes of the woodpile structure.

are controlled by the oxidation process.[28,29] The conductivity peak at 13 minutes likely corresponds to an optimal molecular weight and polymer chain connectivity. PEDOT synthesized using $FeCl_3$ oxidation possesses a high molecular weight, which contributes to better conductivity. However, prolonged oxidation beyond 13 minutes led to a decline in conductivity, reaching 485 S m^{-1} after 17 minutes. This decrease was attributed to the hydration-induced swelling of the PEGDA/AAc polymer network in the aqueous solution, which enlarged the network's pores, causing the large cross-sectional area S and the exudation of oxidized PEDOT nanofibrils from the matrix. Consequently, the overall PEDOT content reduced, and therefore, conductivity fell. Subsequently, a nanowire resistor was fabricated between gold electrodes *via* DLW technique. Its electrical conductivity was characterized after the oxidation treatment. The resulting current–voltage (i–v) characteristics are shown in Fig. 3(e), yielding a measured resistance of 1.26×10^6 Ω. With an effective length between electrodes of 80 μm and line width of 488 nm, yielded a calculated electrical conductivity of 679 S m^{-1}.

The poly(acrylic acid) (PAAc) network, which forms the structural scaffold of the micro/nanostructures, exhibits excellent pH-responsive swelling and contraction that directly modulates the electrical conductivity of the composite. This behavior originates from the anionic polymer network's strongly hydrophilic carboxyl groups (–COOH). Under alkaline conditions, these groups deprotonate to form carboxylate anions ($–COO^-$), increasing negative charge density and enhancing electrostatic repulsion between polymer chains. This forces the chains apart, leading to volume expansion and pronounced swelling, while the increased density of $–COO^-$ groups also promote additional hydrogen bonding with water molecules, further amplifying water uptake and swelling. Conversely, in acidic environments, the carboxylate anions are progressively protonated back to neutral –COOH groups. This reduces negative charge density, diminishes electrostatic repulsion, allows polymer chains to move closer together, and decreases hydrogen bonding with water, collectively resulting in volume contraction and water expulsion. To quantitatively correlate this pH-dependent dimensional change with the resultant electrical properties, the volumetric behavior was first characterized across a range of acidic and alkaline conditions.

A woodpile structure with an expected length of 40 μm and height of 12 μm was fabricated. Immersion in deionized water for 5 h allowed the polymer material to fully hydrate, inducing significant swelling and expanding the structure to a side length of 47.3 μm (Fig. 4(d)). To investigate its behavior under acidic conditions, this hydrated/swollen structure was immersed in HNO_3 solutions of varying pH, and its dimensional changes were monitored. After immersion in a pH = 5 HNO_3 solution for 1 h, the side length contracted to 44.4 μm. Subsequent transfer to a pH = 3 HNO_3 solution for an additional 1 h resulted in further contraction to 41.4 μm. Finally, immersion in an extreme acidic environment (pH = 1) for 1 h caused a marginal contraction to 40.7 μm (Fig. 4(a–c)). Conversely, after rinsing and rehydrating in deionized water, immersion in a pH = 9 NaOH solution for 1 h caused the side length to swell from 47.3 μm to 49.7 μm. Transfer to a stronger alkaline environment (pH = 11) for 1 h induced further expansion to 52.4 μm, and finally, immersion in an extreme alkaline solution (pH = 13) for 1 h resulted in the maximum side length of 53.5 μm (Fig. 4(e–g)). The dimensions of the woodpile structure under different pH environments are shown in Fig. 4(h). The dimensional response of the structure exhibited a clear dependence on environmental pH: under acidic conditions, increasing acidity progressively contracted the structure, while under alkaline conditions, increasing alkalinity induced significant swelling. Within the

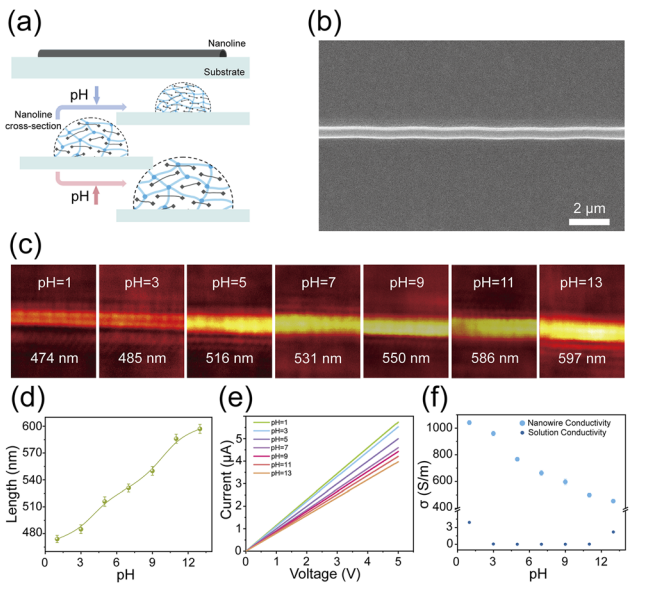

Fig. 5 Variations in dimensions and electrical conductivity of the nanowires under different pH conditions. (a) Schematic illustration of the contraction and expansion of the polymer network within the nanowire structure under varying pH conditions. (b) SEM images of the nanowire. (c) Confocal microscopy images of the nanowire under different pH conditions. (d) Variation in nanowire width under different pH conditions. (e) I–V curve of the nanowire under different pH conditions. (f) Electrical conductivity of the nanowire structure at different pH values and the corresponding solutions.

pH ranging from 3 to 11, the dimensional changes followed an approximately linear relationship with pH. At the extreme acidity of pH = 1, the structure contracted to its minimum size of 40.7 μm.

In order to further explore the influence of the swelling/contraction of the nanostructure under pH stimuli, as illustrated in Fig. 5(a), a nanowire structure was fabricated to characterize the relationship between cross-sectional area and electrical conductivity. The SEM image in Fig. 5(b) depicts a representative nanowire. After sequential immersion and equilibration in solutions of varying pH, the pH-responsive dimensional changes of the polymer wire were quantified using confocal microscopy (Fig. 5(c)). When the pH = 1, the line width contracted to 474 nm. It then increased monotonically with rising pH, reaching 597 nm at pH = 13. This volumetric change directly modulates electrical conductivity. Current–voltage (*I–V*) measurements (Fig. 5(e)) reveal that the calculated conductivity (Fig. 5(f)) increases under acidic conditions and decreases under alkaline conditions. It should be noted that the intrinsic conductivities of the pH = 1 and pH = 13 solutions are 3.9 S m^{-1} and 2.2 S m^{-1}, respectively, which are negligible compared to the measured values of the nanostructure and thus do not compromise the validity of the conductivity results. Specifically, the conductivity reaches 1041 S m^{-1} at pH = 1, compared to 663 S m^{-1} at pH = 7 and 454 S m^{-1} at pH = 13. The underlying mechanism of this phenomenon originates from a multilevel structural response and reorganization within the material, orchestrated by pH regulation. In acidic environments, the PAAc network contracts and densifies the matrix through protonation. This process not only reduces the interchain distances within the conductive PEDOT network but also drives conformational reconstruction and microstructural ordering of the PEDOT chains themselves.[30,31] Specifically, the protonating environment induces a transformation of the PEDOT chains from their initial, lower-energy "coil-like" benzoid structure with weaker conjugation to an "extended" quinoid structure possessing higher conjugation length and superior charge delocalization capability, thereby significantly enhancing their intrinsic charge transport capacity. Simultaneously, following post-acid treatment, the more regularized PEDOT chains can assemble more effectively, forming conductive pathways with a higher degree of alignment and order. Consequently, acid treatment enhances charge transport efficiency not merely by compressing the matrix to reduce physical transport distances but, more fundamentally, by optimizing the molecular conformation and long-range ordering of the conductive filler. Conversely, in alkaline environments, ionization of PAAc induces electrostatic repulsion and network expansion, creating greater barriers for charge transport and diminishing conductivity. The observed geometric cross-sectional changes further contribute to the magnitude of the calculated conductivity shifts.

Conclusions

We developed a composite photoresist doped with EDOT for the fabrication of 3D micro/nanostructures *via* DLW technique. Post chemical oxidation converts the polymerized network into a conductive PEDOT matrix. The resulting structures exhibit a feature size of 250 nm. These structures exhibit pH-responsive behavior, allowing their electrical conductivity to be reversibly modulated from 679 S m^{-1} to a range of 454 S m^{-1} at pH = 13 and 1041 S m^{-1} at pH = 1, in tandem with corresponding line width changes from 488 nm to 597 nm and 474 nm, respectively. This performance demonstrates the efficacy of our method for producing high-quality PEDOT nanostructures. This approach provides a viable pathway for implementing PEDOT in advanced tunable nanodevices, with particular promise for applications such as biosensing and neuromorphic computing systems.

Author contributions

Qingbin Zhou: conceptualization, investigation, data curation, formal analysis, methodology, writing – original draft. Yucheng Long: investigation, data curation, formal analysis, methodology. Shichao Song: writing – original draft, writing – review & editing, supervision. Zilan Deng: funding acquisition, writing – review & editing. Xiangping Li: Resources, writing – review & editing, supervision. Yaoyu Cao: funding acquisition, writing – review & editing, supervision.

Conflicts of interest

The authors have no conflicts to disclose.

Data availability

The data that support the findings of this study are available within the article.

Acknowledgements

This work was supported by National Natural Science Foundation of China (62422506, 62275108).

References

1 G. Arias-Ferreiro, A. Ares-Pernasa, M. S. Dopico-Garcíaa, A. Lasagabáster-Latorre and M.-J. Abada, *Eur. Polym. J.*, 2020, **136**, 109887.
2 C. Song, Q. Zhao, T. Xie and J. Wu, *J. Mater. Chem. A*, 2024, **12**, 5348.
3 C.-Y. Yang, M.-A. Stoeckel, T.-P. Ruoko, H.-Y. Wu, X. Liu, N. B. Kolhe, Z. Wu, Y. Puttisong, C. Musumeci, M. Massetti, H. Sun, K. Xu, D. Tu, W. M. Chen, H. Y. Woo, M. Fahlman, S. A. Jenekhe, M. Berggren and S. Fabiano, *Nat. Commun.*, 2021, **12**, 2354.
4 J. Rivnay, S. Inal, B. A. Collins, M. Sessolo, E. Stavrinidou, X. Strakosas, C. Tassone, D. M. Delongchamp and G. G. Malliaras, *Nat. Commun.*, 2016, **7**, 11287.
5 O. Dadras-Toussi, M. Khorrami, A. S. C. L. S. Titus, S. Majd, C. Mohan and M. R. Abidian, *Adv. Mater.*, 2022, **34**, 2200512.
6 J. Li, J. Cao, B. Lu and G. Gu, *Nat. Rev. Mater.*, 2023, **8**, 604.

7 Y. Jiang, Z. Zhang, Y.-X. Wang, D. Li, C.-T. Coen, E. Hwaun, G. Chen, H.-C. Wu, D. Zhong, S. Niu, W. Wang, A. Saberi, J.-C. Lai, Y. Wu, Y. Wang, A. A. Trotsyuk, K. Y. Loh, C.-C. Shih, W. Xu, K. Liang, K. Zhang, Y. Bai, G. Gurusankar, W. Hu, W. Jia, Z. Cheng, R. H. Dauskardt, G. C. Gurtner, J. B.-H. Tok, K. Deisseroth, I. Soltesz and Z. Bao, *Science*, 2022, **375**, 1411.

8 Y.-Q. Zheng, Y. Liu, D. Zhong, S. Nikzad, S. Liu, Z. Yu, D. Liu, H.-C. Wu, C. Zhu, J. Li, H. Tran, J. B.-H. Tok and Z. Bao, *Science*, 2021, **373**, 88.

9 V. R. Feig, H. Tran, M. Lee, K. Liu, Z. Huang, L. Beker, D. G. Mackanic and Z. Bao, *Adv. Mater.*, 2019, **31**, 1902869.

10 S. Tagliaferri, A. Panagiotopoulos and C. Mattevi, *Mater. Adv.*, 2021, **2**, 540.

11 D. Mawad, E. Stewart, D. L. Officer, T. Romeo, P. Wagner, K. Wagner and G. G. Wallace, *Adv. Funct. Mater.*, 2012, **22**, 2692.

12 L. Pan, G. Yu, D. Zhai, H. R. Lee, W. Zhao, N. Liu, H. Wang, B. C.-K. Tee, Y. Shi, Y. Cui and Z. Bao, *Proc. Natl. Acad. Sci. U. S. A.*, 2012, **109**, 9287.

13 J. Liu, J. Garcia, L. M. Leahy, R. Song, D. Mullarkey, B. Fei, A. Dervan, I. V. Shvets, P. Stamenov, W. Wang, F. J. O'Brien, J. N. Coleman and V. Nicolosi, *Adv. Funct. Mater.*, 2023, **33**, 2214196.

14 H. Yuk, B. Lu, S. Lin, K. Qu, J. Xu, J. Luo and X. Zhao, *Nat. Commun.*, 2020, **11**, 1604.

15 B. Lu, H. Yuk, S. Lin, N. Jian, K. Qu, J. Xu and X. Zhao, *Nat. Commun.*, 2019, **10**, 1043.

16 B. Oh, S. Baek, K. S. Nam, C. Sung, C. Yang, Y.-S. Lim, M. S. Ju, S. Kim, T.-S. Kim, S.-M. Park, S. Park and S. Park, *Nat. Commun.*, 2024, **15**, 5839.

17 S. Kawata, H.-B. Sun, T. Tanaka and K. Takada, *Nature*, 2001, **412**, 697.

18 Z. Gan, Y. Cao, R. A. Evans and M. Gu, *Nat. Commun.*, 2013, **4**, 2061.

19 C. Andrea, P. Luana, F. Maria and P. Dario, *Adv. Opt. Mater.*, 2019, **7**, 1800419.

20 S. K. Saha, D. Wang, V. H. Nguyen, Y. Chang, J. S. Oakdale and S.-C. Chen, *Science*, 2019, **366**, 105.

21 S.-Y. Yin, Q. Guo, S.-R. Liu, J.-W. He, Y.-S. Yu, Z.-N. Tian and Q.-D. Chen, *Opto-Electron. Sci.*, 2024, **3**, 240003.

22 L. Li, R. R. Gattass, E. Gershgoren, H. Hwang and J. T. Fourkas, *Science*, 2009, **324**, 910.

23 Q. Jiang, L. Chen, J. Liu, Y. Zhang, S. Zhang, D. Feng, T. Jia, P. Zhou, Q. Wang, Z. Sun and H. Xu, *Opto-Electron. Sci.*, 2023, **2**, 220002.

24 Z. Luo, Y. Liu, Z. Liu, D. Wang, Z. Gan and C. Xie, *Nanotechnology*, 2020, **31**, 255301.

25 K. Kurselis, R. Kiyan, V. N. Bagratashvili, V. K. Popov and B. N. Chichkov, *Opt. Express*, 2013, **21**, 31029.

26 S. Hou, H. Chen, D. Lv, W. Li, X. Liu, Q. Zhang, X. Yu and Y. Han, *ACS Appl. Mater. Interfaces*, 2023, **15**, 28503.

27 D. Ludescher, P. Ruchka, L. Siegle, Y. Huang, P. Flad, M. Ubl, S. Ludwigs, M. Hentschel and H. Giessen, *Adv. Opt. Mater.*, 2025, **13**, 2403271.

28 Y. Li, B. Gao, Y. Diao, H. Xiang, J. Yao, X. Xu, Q. Li, X. Wang, X. Li, F. Wang, D. Yang, H. Lou and R. Yang, *Adv. Mater.*, 2025, **37**, 2502394.

29 Q. Fu, Y. Li, X. Wang, Q. Li, F. Wang and R. Yang, *J. Mater. Chem. C*, 2020, **8**, 17185.

30 Z. Guo, J. Tang, J. Yao and Y. Li, *Polym. Chem.*, 2024, **15**, 2191.

31 B. Adilbekova, A. D. Scaccabarozzi, H. Faber, M. I. Nugraha, V. Bruevich, D. Kaltsas, D. R. Naphade, N. Wehbe, A.-H. Emwas, H. N. Alshareef, V. Podzorov, J. Martín, L. Tsetseris and T. D. Anthopoulos, *Adv. Mater.*, 2024, **36**, 2405094.